Supporting Information for:

Asymmetric bis-PNP pincer complexes of Zirconium and Hafnium - a measure of hemilability

Celia Idelson,[a] Leah Webster[a] Tobias Krämer,[b] F. Mark Chadwick[a]**

Department of Chemistry, Molecular Sciences Research Hub, Imperial College London, White City, Shepherds Bush, London, W12 0BZ, UK. E-mail: m.chadwick@imperial.ac.uk.

Department of Chemistry, Maynooth University, Maynooth, Co. Kildare, Ireland. E-mail: tobias.kraemer@mu.ie.

Contents

1. Experimental Details and Syntheses

1.1 General Considerations

Unless otherwise stated all manipulations were carried out under an inert atmosphere (N_2) using standard dual-manifold Schlenk techniques or employment of an MBraun Labmaster glovebox. Glassware were dried in an oven at 150°C overnight before use. Anhydrous solvents (toluene, pentane, CH_2Cl_2) were obtained from a Grubbs type SPS system and stored over activated 3 Å molecular sieves (CH_2Cl_2) or potassium mirrors (toluene, benzene, pentane) under inert atmosphere. THF and Et_2O were dried by refluxing over Na/Fluorenone and stored over activated 3 Å molecular sieves or potassium mirror respectively, whilst being kept under inert atmosphere. All other solvents, including deuterated solvents, were dried by being stored over activated 3 Å molecular sieves and subsequent degassing by three freeze-pump-thaw cycles. Elemental analyses were recorded by MEDAC ltd.

Solution NMR data were collected on either a Brucker 400 MHz or 500 MHz spectrometer employing NMR tubes fitted with a J. Young's style stopcock. Data were collected at room temperature unless stated otherwise. Variable temperature data were collected by Mr Pete Haycock. Chemical shifts (δ) are stated in PPM and referenced internally to residual solvent protio-resonances (^{1}H) or externally to 85% H_3PO_4 (^{31}P) or LiCl (^{7}Li). Coupling constants (J) are quoted in Hz. The data was processed using Mestrenova.

Single crystal X-ray diffraction data were collected as follows: a typical crystal was mounted on a MiTeGen Micromounts using perfluoropolyether oil and cooled rapidly to 173 K in a stream of nitrogen gas using a cryostream unit. Data were collected with an Agilent Diffraction Xcalibur PX Ultra A and Xcalibur 3 E diffractometers (Cu Kα radiation, λ = 1.54180 Å). Raw frame data were reduced using CrysAlisPro.[1] The structures were solved using SuperFlip and refined using full-matrix least squares refinement on all F^2 data using the CRYSTALS program suite.[2–4] In general distances and angles were calculated using the full covariance matrix.

$ZrCl_4$·2THF, $HfCl_4$·2THF and 2,5-bis(dimethylaminomethyl)pyrrole were prepared by literature procedures.[5,6] **[PNP^{Ph}]Li·Et$_2$O** was made by an adapted literature procedure which is given below.[7,8,17,9–16] All other chemicals were obtained from commercial suppliers (Sigma-Aldrich, Fluorochem, TCI).

1.2 Synthesis of [PNP^{Ph}]Li·Et$_2$O

A Schlenk flask was charged with 2,5-bis(dimethylaminomethyl)pyrrole in toluene (1.82 M, 5.5 mL, 10 mmol) and the solvent removed *in vacuo* to yield an orange oil. Diphenylphosphine (3.5 mL, 20 mmol) was added and the reaction mixture was stirred at 150°C for 22 h to yield a viscous yellow oil. This was aliquoted to ensure full conversion and if necessary further 2,5-bis(dimethylaminomethyl)pyrrole was added. **[PNP^{Ph}]H** was used directly in future reactions without purification. Crude **[PNP^{Ph}]H** was dissolved in toluene (c. 20 mL), and cooled to -78°C. ^{n}BuLi (2.5 M in hexane, 4.5 mL, 11 mmol) was added dropwise at -78°C to form a deep orange solution. The solution was stirred at RT for 1 h, forming a precipitate. The solvent was removed in vacuo, and taken up in Et_2O (20 mL). The solution was filtered via cannula and then pentane was added (150 mL) yielding a orange/red precipitate which can be isolated and washed with further pentane (3 × 50 mL) and dried under vacuum (4.01 g, 8.5 mmol, 86%). Crystals of the THF adduct suitable for X-ray diffraction could be grown by layering THF solution with pentane. ^{1}H NMR (400 MHz, C_6D_6) δ: 7.16-7.01 (br m, 20H, phenyl CH), 6.29 (s, 2H, pyr-CH), 3.31 (s, 4H, CH_2PPh_2), 3.26 (q, 4H, Et_2O), 1.11 (t, 6H, Et_2O). ^{7}Li NMR (400 MHz, C_6D_6) δ: -3.5 (s). ^{31}P{^{1}H}

NMR (202 MHz, C_6D_6) δ: −18.4 (s). CHN elemental analysis found C 74.8 H 6.5 N 2.9 calculated for $C_{34}H_{36}LiNOP_2$: C 75.1 H 6.7 N 2.6 %

1.3 Synthesis of $[PNP^{Ph}]_2ZrCl_2$

Benzene (c. 10 mL) solutions of **$[PNP^{Ph}]Li{\cdot}Et_2O$** (2.503 g, 4.60 mmol) and $ZrCl_4{\cdot}2THF$ (0.701 g, 1.84 mmol) were prepared. The solutions were combined, immediately forming a dark orange solution. The solution was stirred at RT for 1 h, in which time the solution brightened, and a precipitate formed. The solution was filtered to yield a clear orange solution, and the solvent was removed *in vacuo* to yield an orange residue. The solution was dissolved in dichloromethane (c. 20 mL) to yield a red solution, which was filtered and dried *in vacuo* to yield an orange solid. The solid was dissolved in THF (5 mL) and pentane (40 mL) was added until a precipitate was yielded. The solution was removed via cannula and the powder was washed with pentane (15 mL x 3). The remaining solvent was removed *in vacuo* to yield a free-flowing orange powder (1.480 g, 1.36 mmol, 74%). Crystals suitable for X-ray diffraction were grown by layering a saturated THF solution with pentane.
^1H NMR (400 MHz, C_6D_6, 298 K) δ: 7.34 (br s, 5H, phenyl-H), 7.18 (m, 10H, phenyl-H), 7.02 (br s, 11H, phenyl-H), 6.91 (m, 9H, phenyl-H), 6.77 (m, 5H, phenyl-H), 6.20 (br s, 2H, pyr-H), 6.01 (br s, 2H, pyr-H), 4.56 (d, 2H, CH_2PPh_2), 3.64 (br, 2H, CH_2PPh_2), 3.46 (br, 2H, CH_2PPh_2). $^{31}P\{^1H\}$ NMR (202 MHz, C_6D_6) δ: 13.4 (s). $^{31}P\{^1H\}$ NMR (202 MHz, 203 K, C_6D_6) δ: 16.3 (d of d), 15.0-14.8 (m), −15.2 (s) $^{31}P\{^1H\}$ $T_{coalescence}$: 249 K. CHN elemental analysis found C 66.0 H 5.0 N 3.1 calculated for $C_{60}H_{52}Cl_2N_2P_4Zr$: C 66.3 H 4.8 N 2.6 %

1.4 Synthesis of $[PNP^{Ph}]_2HfCl_2$

The synthesis was carried out in an analogous fashion to **$[PNP^{Ph}]_2ZrCl_2$**. Amounts used: **$[PNP^{Ph}]Li{\cdot}Et_2O$** (1.152 g, 2.14 mmol) and $HfCl_4{\cdot}2THF$ (0.515 g, 1.11 mmol). Yield of **$[PNP^{Ph}]_2HfCl_2$**: 0.469 g, 0.40 mmol, 34%. Crystals suitable for X-ray diffraction were grown by layering a saturated THF solution with pentane.
^1H NMR (400 MHz, 293 K, C_6D_6) δ: 7.35 (br s, 5H, phenyl-H), 7.20 (m, 5H, phenyl-H), 7.05 (m, 10H, phenyl-H), 6.94 (m, 5H, phenyl-H), 6.88 (m, 3H, phenyl-H), 6.76 (m, 5H, phenyl-H), 6.21 (br s, 4H, pyr-H), 4.60 (d, 4H, CH_2PPh_2). $^{31}P\{^1H\}$ NMR (202 MHz, 293 K, C_6D_6) δ: 15.9 (s). $^{31}P\{^1H\}$ NMR (202 MHz, 203 K, C_6D_6) δ: 20.8 (d of d), 18.0 (d of d), 15.8 (t), −15.1 (s). $^{31}P\{^1H\}$ $T_{coalescence}$: 270 K CHN elemental analysis found C 61.6 H 4.9 N 2.8 calculated for $C_{60}H_{52}Cl_2N_2P_4Hf$: C 61.4 H 4.5 N 2.4 %

2. Further X-ray Crystallographic Details

2.1 Structure of $[PNP^{Ph}]_2HfCl_2$

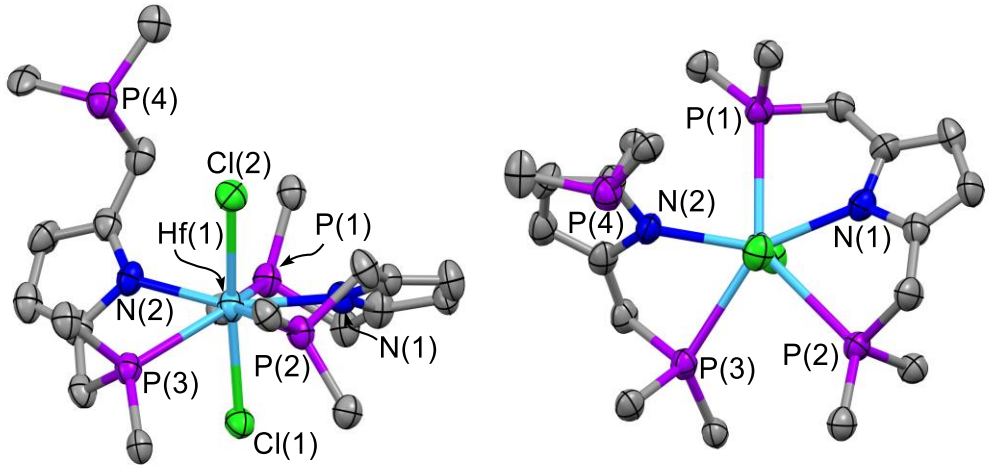

Figure S1: The single crystal X-ray structure of **$[PNP^{Ph}]_2HfCl_2$**. Thermal probability ellipsoids at 50%, hydrogen, non-ipso phenyl carbons and one disordered phenyl ring omitted for clarity.

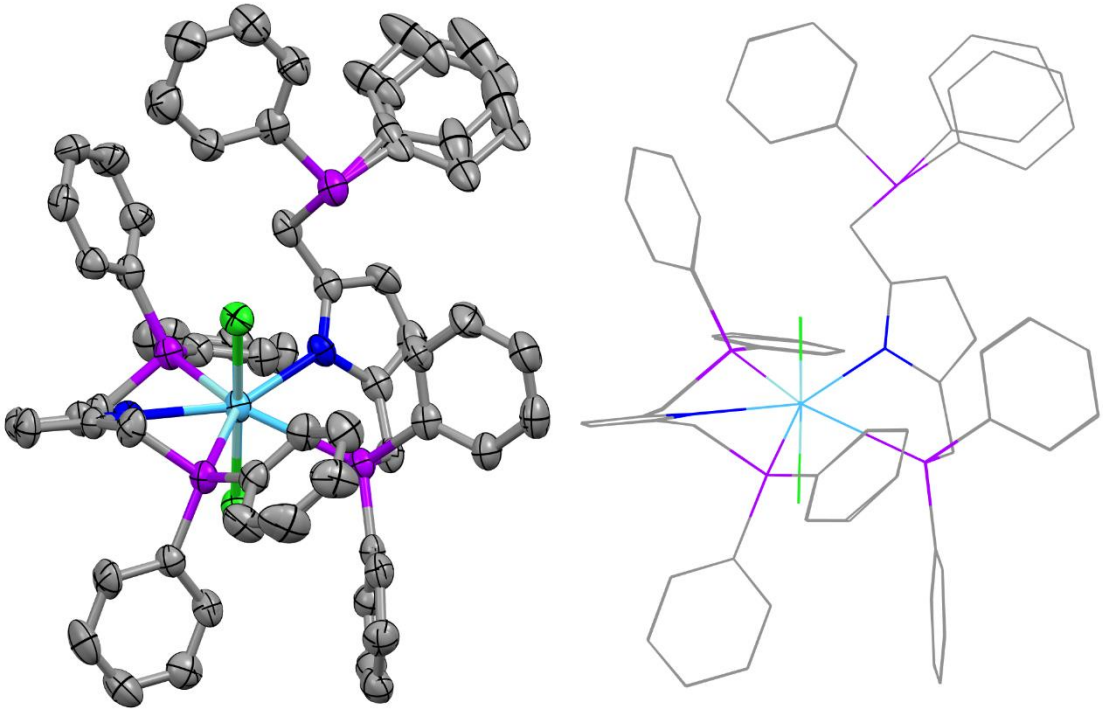

Figure S2: Overlay of the single crystal X-ray structures of **$[PNP^{Ph}]_2ZrCl_2$** and **$[PNP^{Ph}]_2HfCl_2$**. Left: Thermal ellipsoids (at 50 % probability), Right: wire-frame. The Zr/Hf centre is defined to be at the same relative atomic co-ordinates.

2.2 Crystallographic Data Tables

	[PNP^{Ph}]$_2$ZrCl$_2$	**[PNP^{Ph}]$_2$HfCl$_2$**	**Li[PNP^{Ph}]·THF**
Crystal data			
Chemical formula	$C_{60}H_{52}Cl_2N_2P_4Zr$	$C_{60}H_{52}Cl_2N_2P_4Hf$	$C_{34}H_{34}LiNOP_2$
M_r	1087.11	1174.38	541.54
Crystal System	Triclinic	Triclinic	Triclinic
Space group	*P* -1	*P* -1	*P* -1
a, *b*, *c* (Å)	11.1053 (7), 13.1355 (8), 20.3905 (10)	11.07535 (3), 13.14605 (3), 20.39291 (4)	10.70733 (3), 10.84431 (3), 14.74442 (3)
α, β, γ (°)	85.224 (4), 86.838 (4), 66.436 (6)	84.873 (4), 86.804 (5), 66.482 (5)	94.396 (4), 105.416 (4), 114.647 (4)
V (Å^3)	2716.2 (3)	2710.96 (10)	1465.32 (8)
μ (mm^{-1})	3.98	5.89	1.55
Crystal size (mm)	0.20 × 0.20 × 0.10	0.20 × 0.20 × 0.10	0.10 × 0.10 × 0.10
Data collection			
T_{min}, T_{max}	0.52, 0.67	0.36, 0.56	0.77, 0.86
No. of measured, independent and observed [$I > 2.0\sigma(I)$] reflections	15595, 10361, 8347	15997, 11605, 8407	8327, 5524, 4372
R_{int}	0.039	0.069	0.027
$(\sin\theta/\lambda)_{max}$ (Å^{-1})	0.622	0.623	0.621
Refinement			
$R[F^2 > 2\sigma(F^2)]$, $wR(F^2)$, *S*	0.045, 0.127, 1.62	0.076, 0.257, 1.59	0.043, 0.101, 1.46
No. of reflections	10316	11601	5524
No. of parameters	622	677	352
No. of restraints	0	140	0
$\Delta\rho_{max}$, $\Delta\rho_{min}$ (e Å^{-3})	0.58, −0.78	3.36, −1.78	0.50, −0.47
CCDC	2023865	2023866	2023867

3 NMR Spectra

3.1 [PNP^{Ph}]Li·Et$_2$O

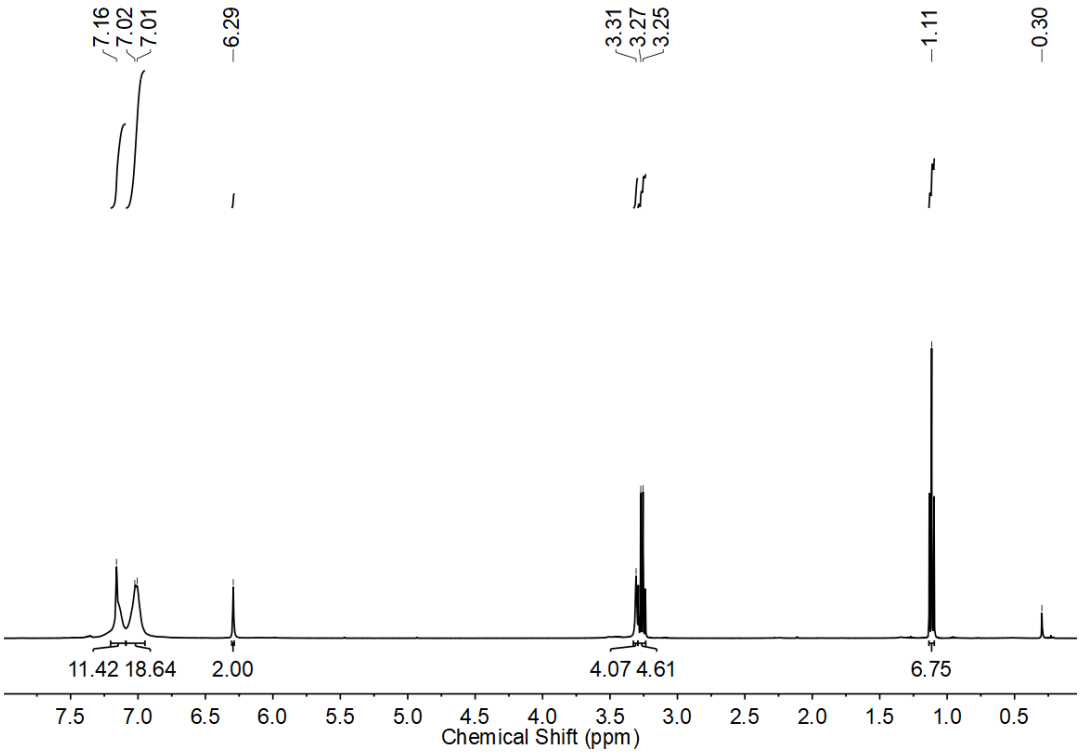

Figure S3: ^{1}H NMR spectrum (C_6D_6, 293 K) of **[PNP^{Ph}]Li·Et$_2$O**.

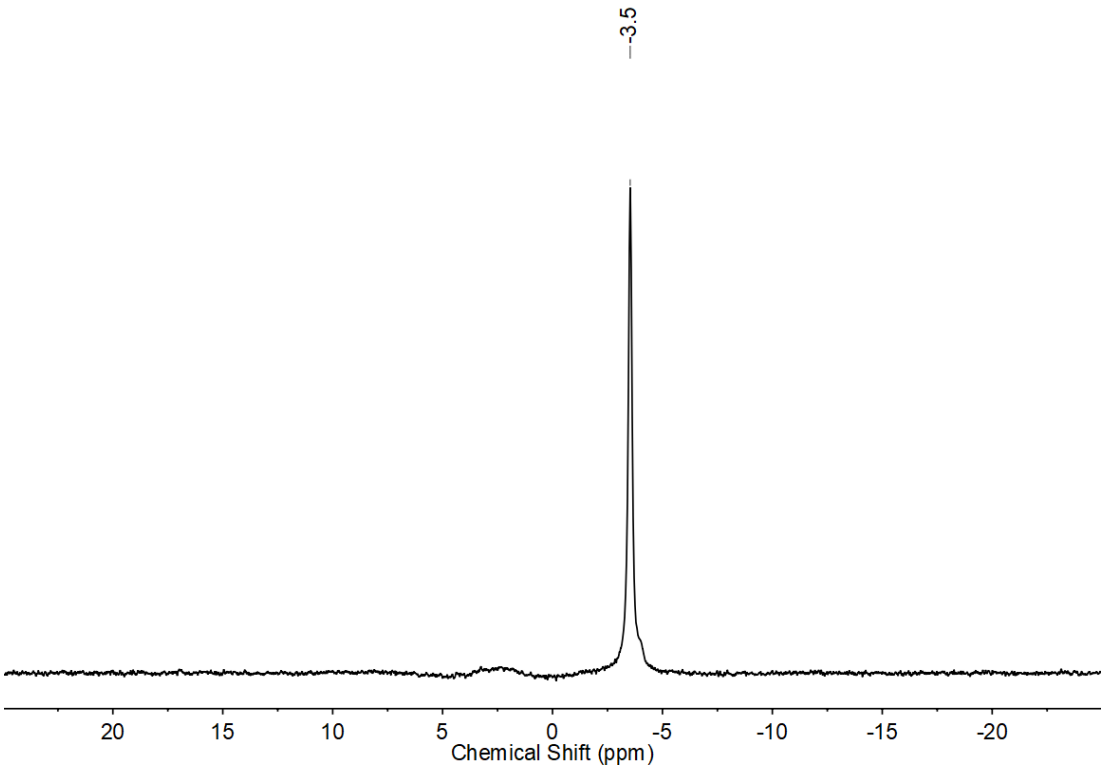

Figure S4: ^{7}Li{^{1}H} NMR spectrum (C_6D_6, 293 K) of **[PNP^{Ph}]Li·Et$_2$O**.

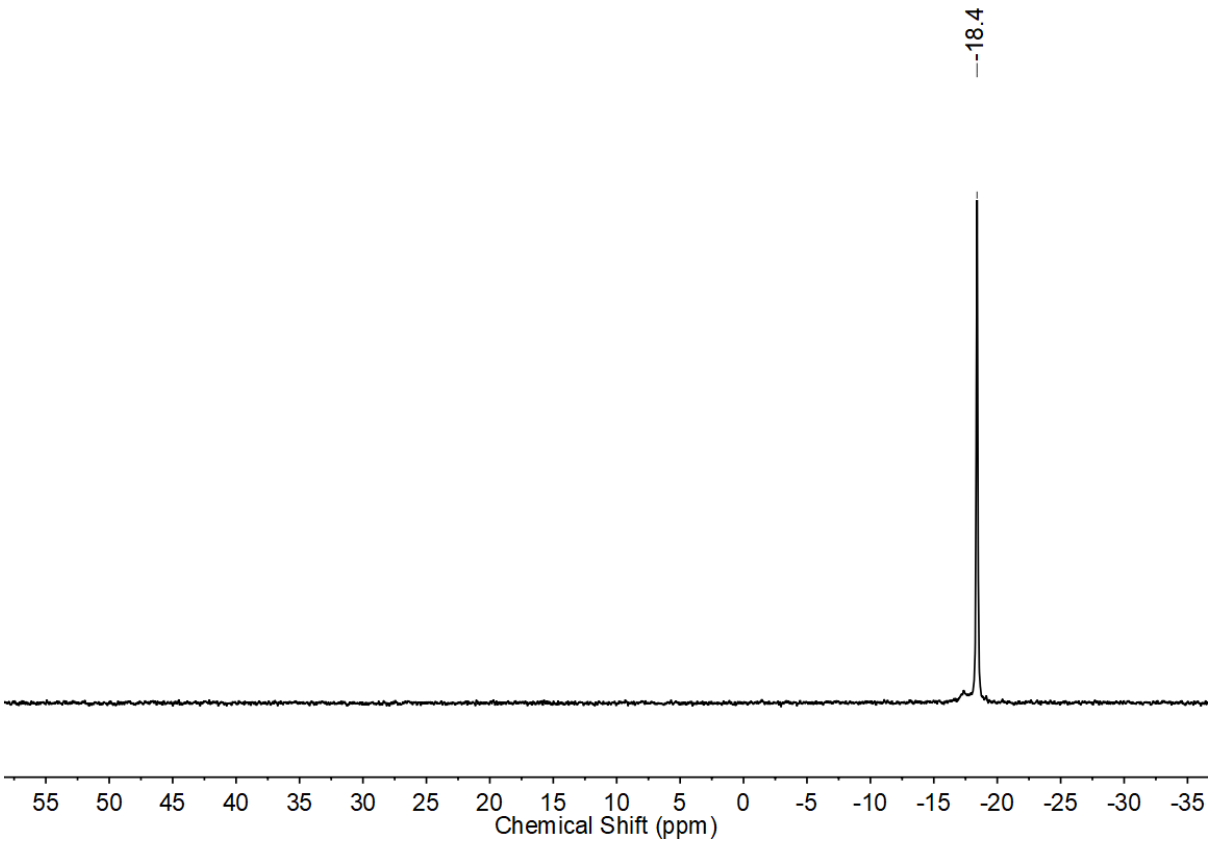

Figure S5: $^{31}P\{^{1}H\}$ NMR spectrum (C_6D_6, 293 K) of **[PNP^{Ph}]Li·Et$_2$O**.

3.2 $[PNP^{Ph}]_2ZrCl_2$

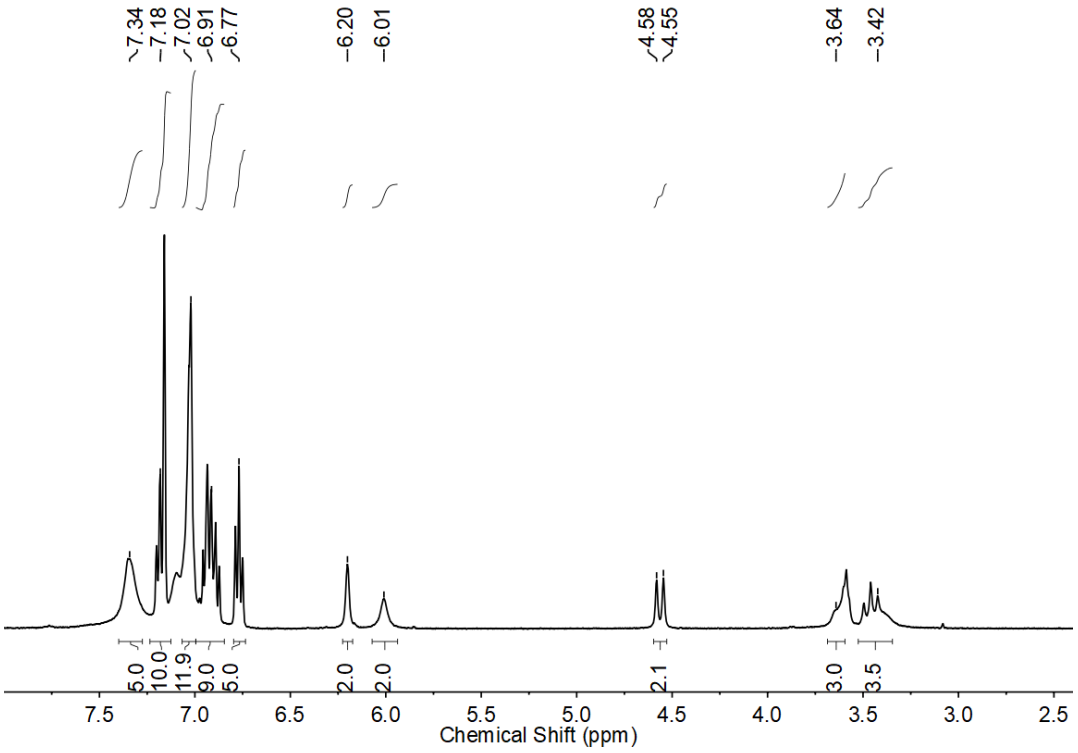

Figure S6: ^{1}H NMR spectrum (C_6D_6, 298 K) of $[PNP^{Ph}]_2ZrCl_2$.

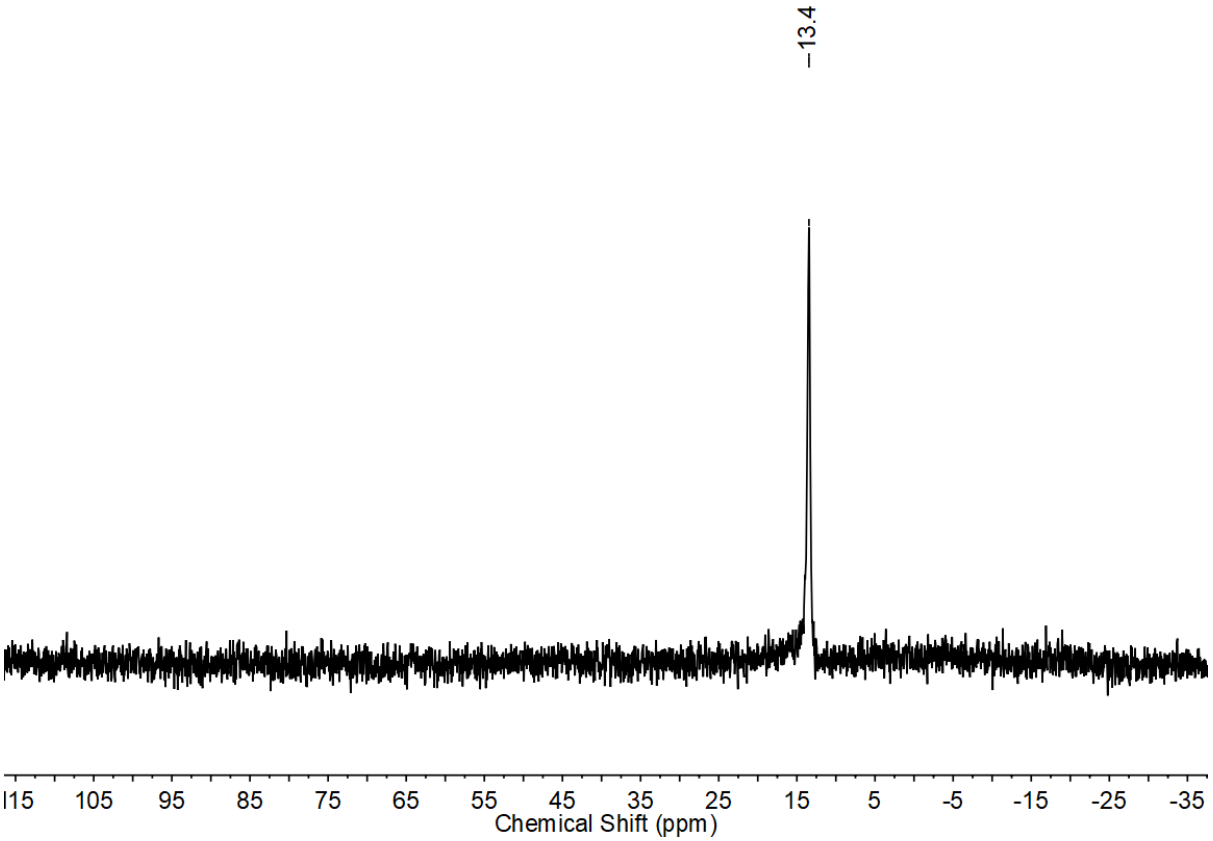

Figure S7: $^{31}P\{^{1}H\}$ NMR spectrum (C_6D_6, 298 K) of $[PNP^{Ph}]_2ZrCl_2$.

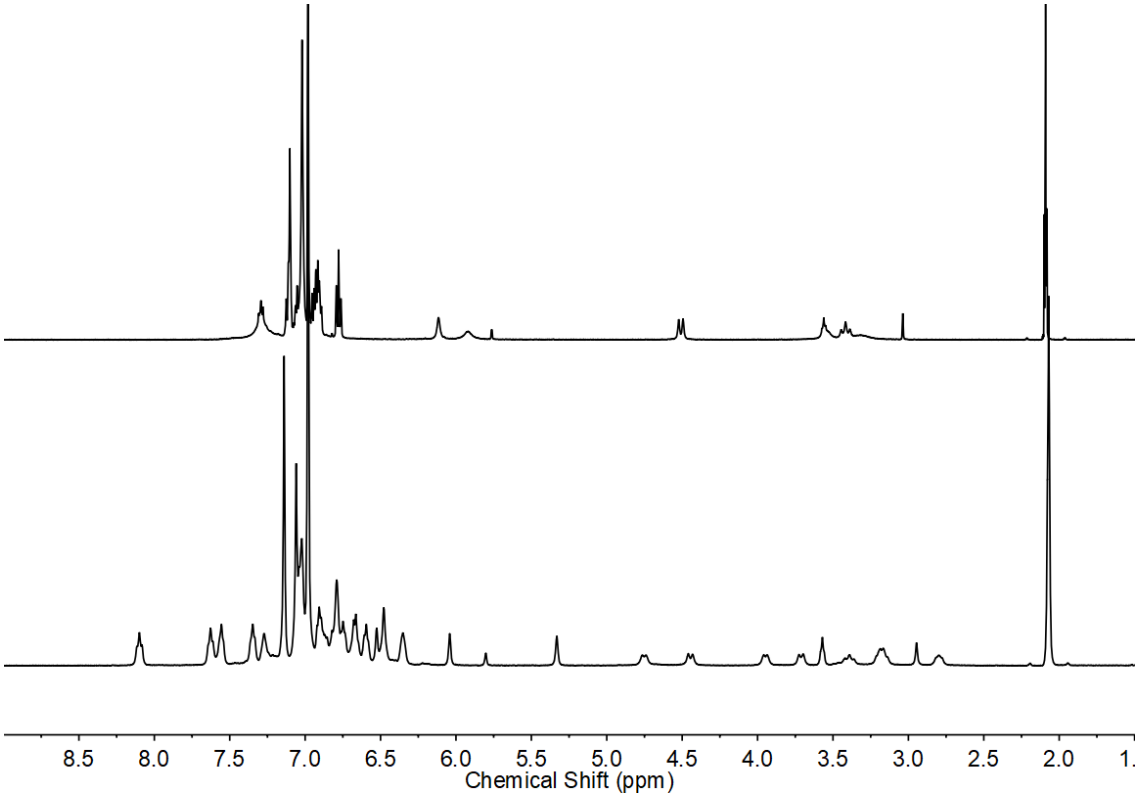

Figure S8*:* ^{1}H NMR spectra (d^{8}-toluene) at 293 K (top) and 203 K (bottom) of **[PNP^{Ph}]$_2$ZrCl$_2$**.

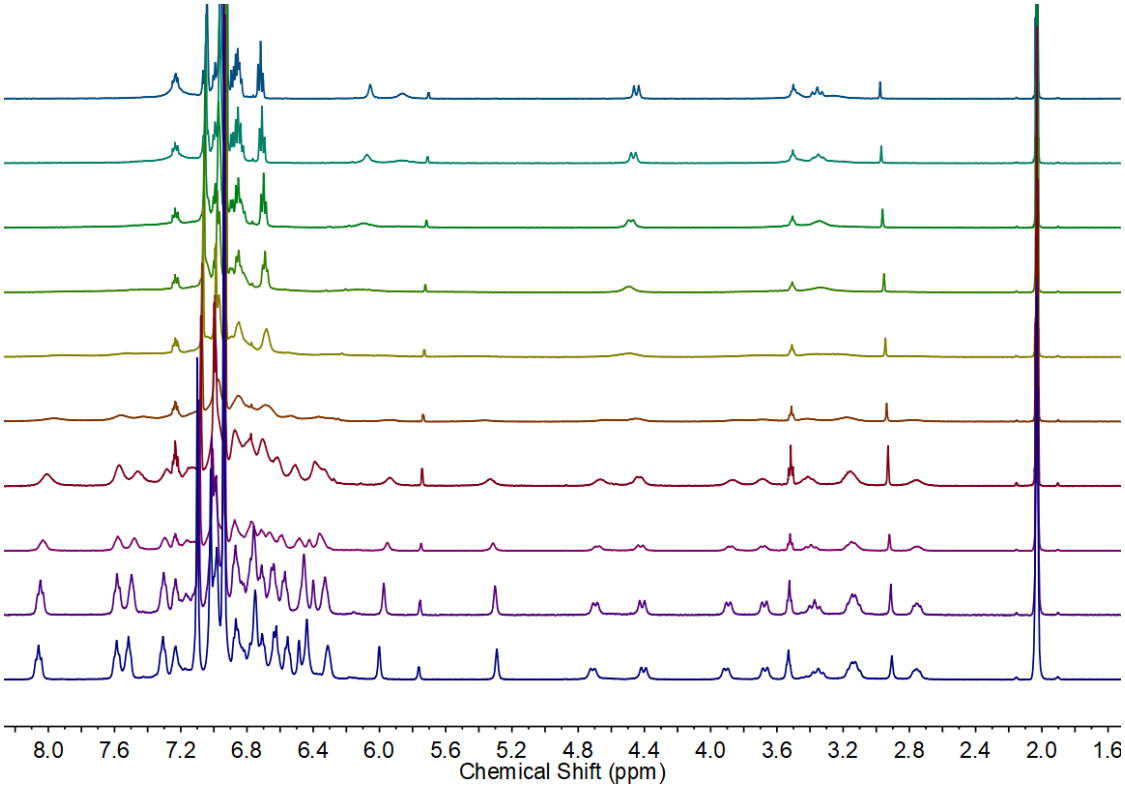

Figure S9: Full variable temperature ^{1}H NMR spectra of **[PNP^{Ph}]$_2$ZrCl$_2$** from 203 K to 293 K in 10 K increments (increasing vertically).

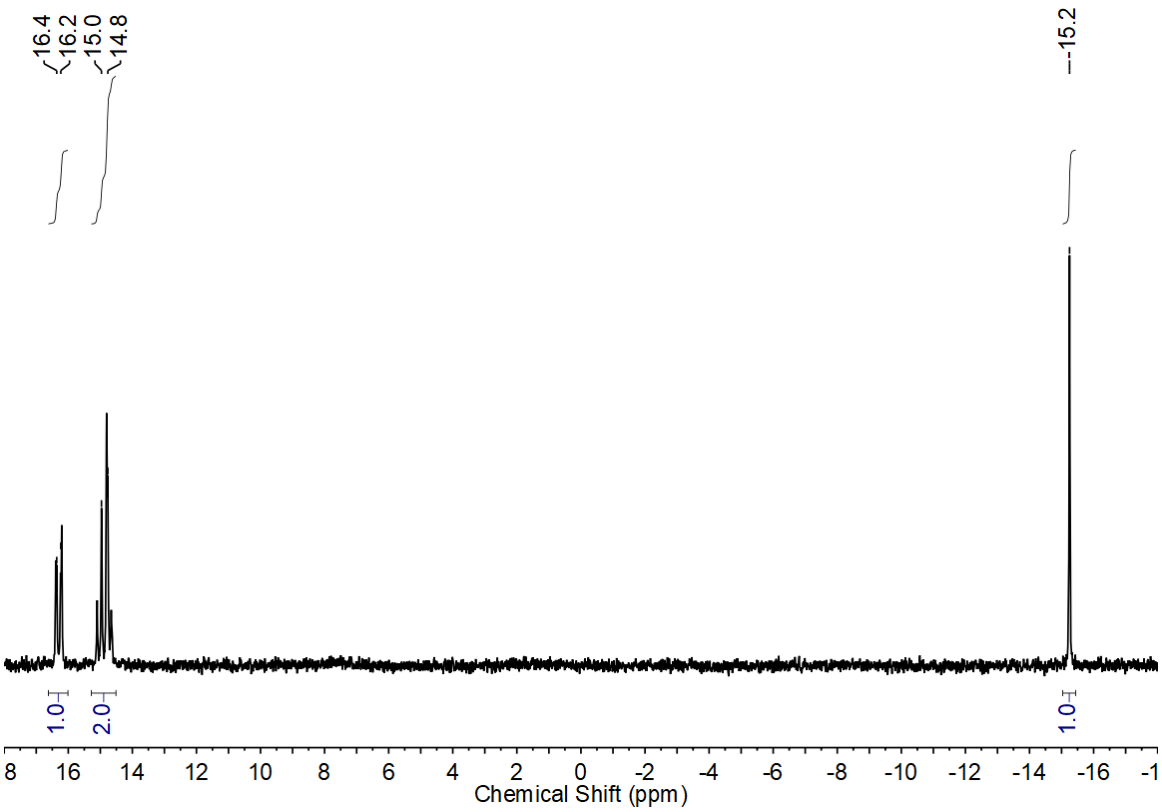

Figure S10: $^{31}P\{^{1}H\}$ NMR spectrum (d^8-toluene) of **[PNP^{Ph}]$_2$ZrCl$_2$** at 203 K.

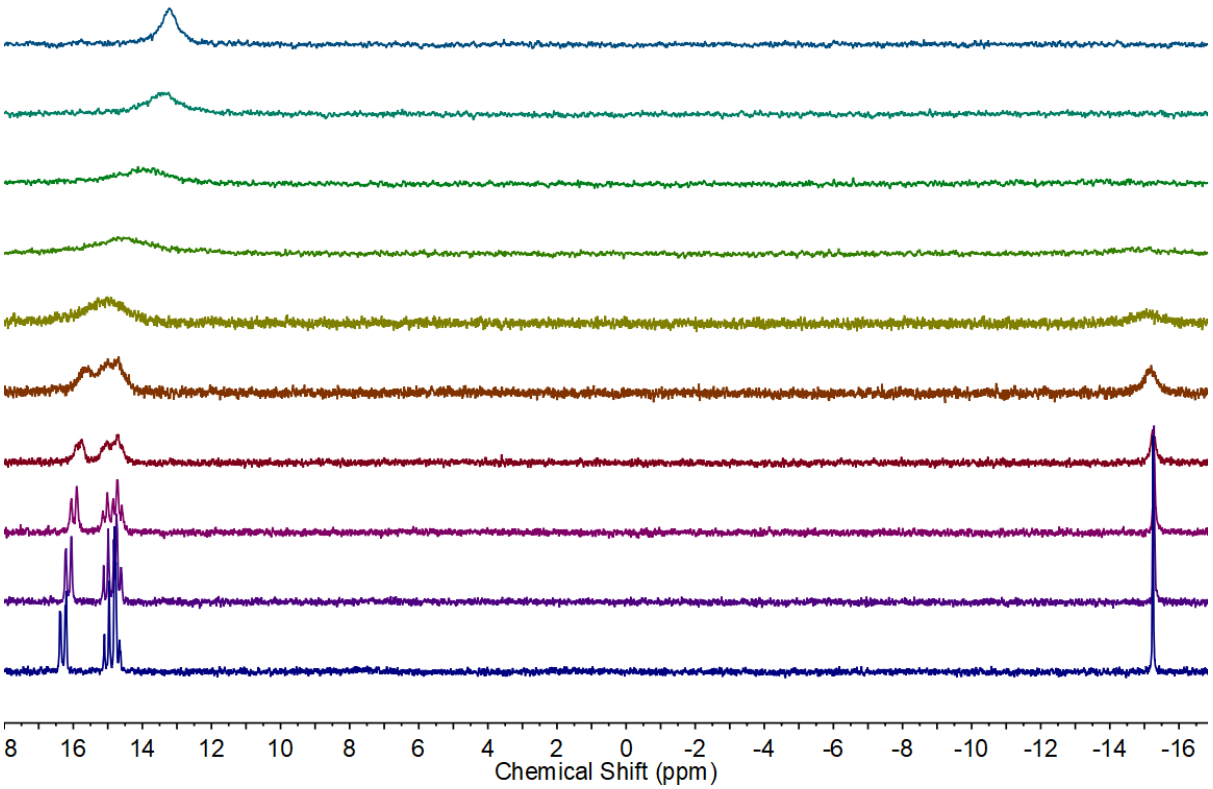

Figure S11: Full variable temperature $^{31}P\{^{1}H\}$ NMR spectra of **[PNP^{Ph}]$_2$ZrCl$_2$** from 203 K to 293 K in 10 K increments (increasing vertically).

3.3 $[PNP^{Ph}]_2HfCl_2$

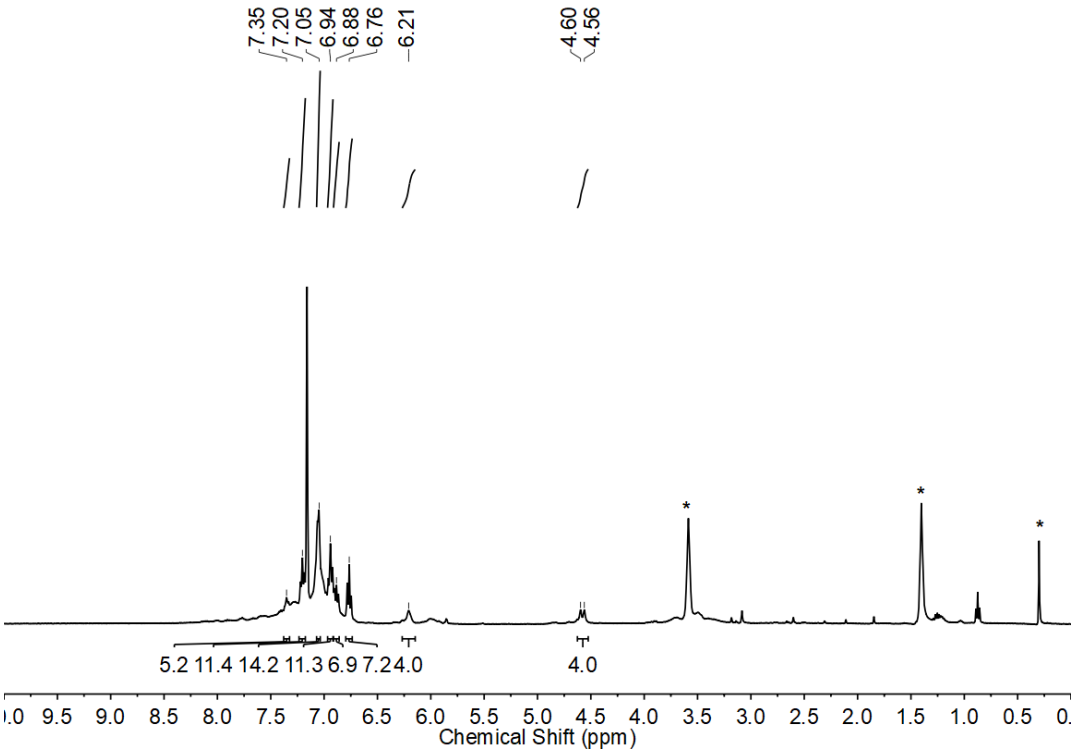

Figure S12: ^{1}H NMR spectrum (C_6D_6, 298 K) of **$[PNP^{Ph}]_2HfCl_2$**. Resonances marked (*) are due to residual Et_2O (from **$[PNP^{Ph}]Li{\cdot}Et_2O$**) and silicon grease.

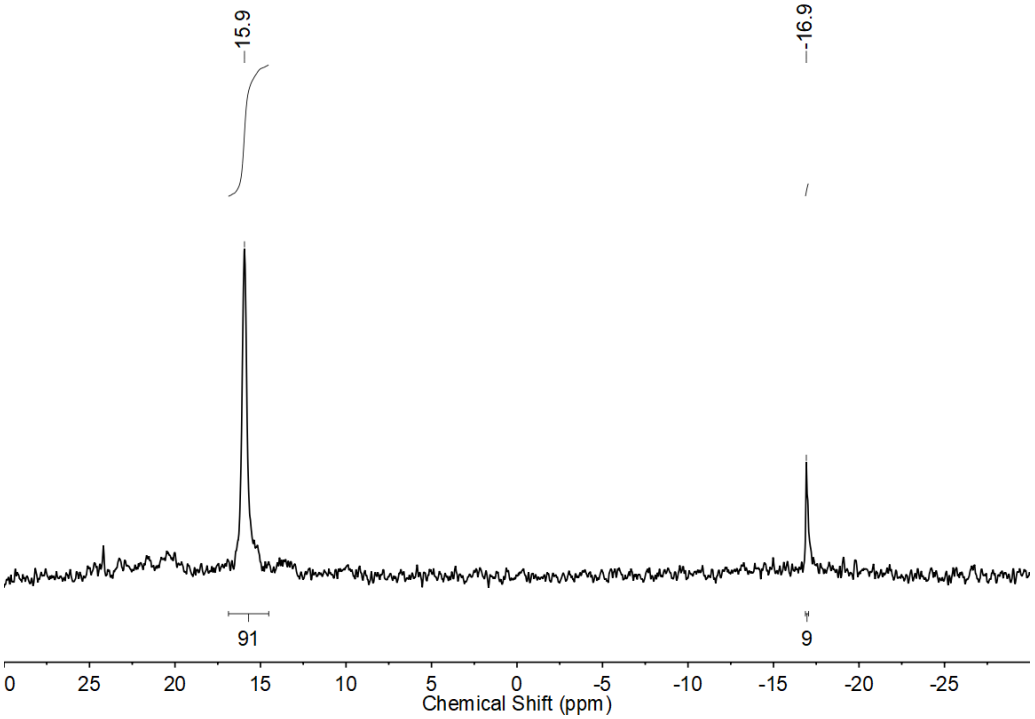

Figure S13: $^{31}P\{^{1}H\}$ NMR spectrum (C_6D_6, 298 K) of **$[PNP^{Ph}]_2HfCl_2$**. The resonance at -16.92 ppm is due to residual of **$[PNP^{Ph}]H$** originating from adventitious water.

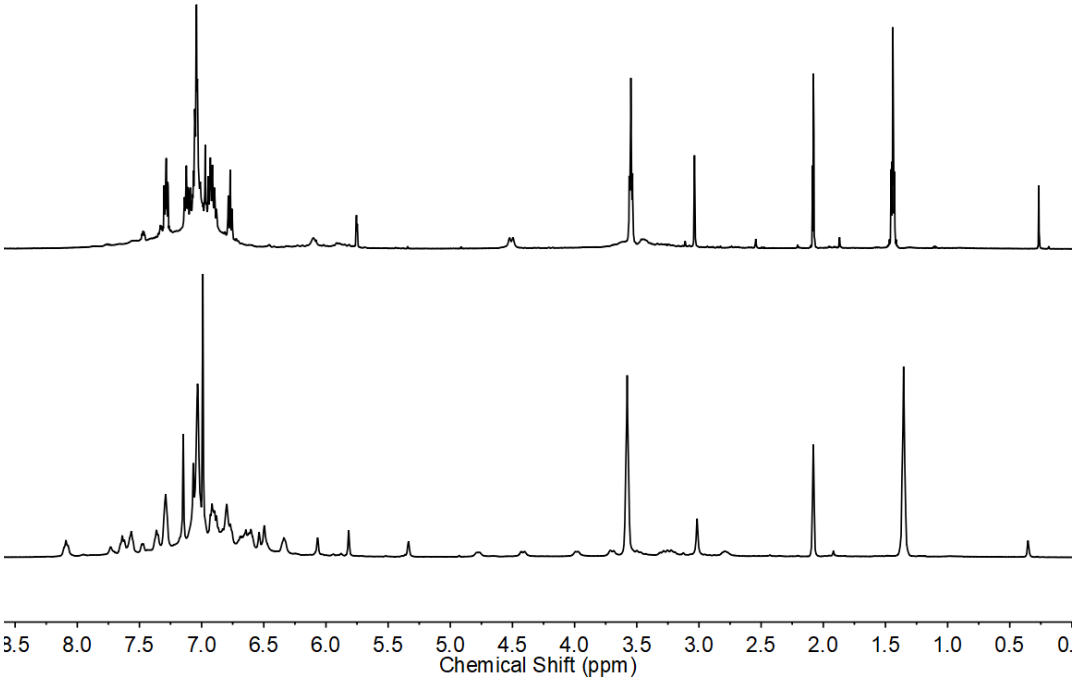

Figure S14: ^{1}H NMR spectra (d^{8}-toluene) at 293 K (top) and 203 K (bottom) of **[PNP^{Ph}]$_2$HfCl$_2$**.

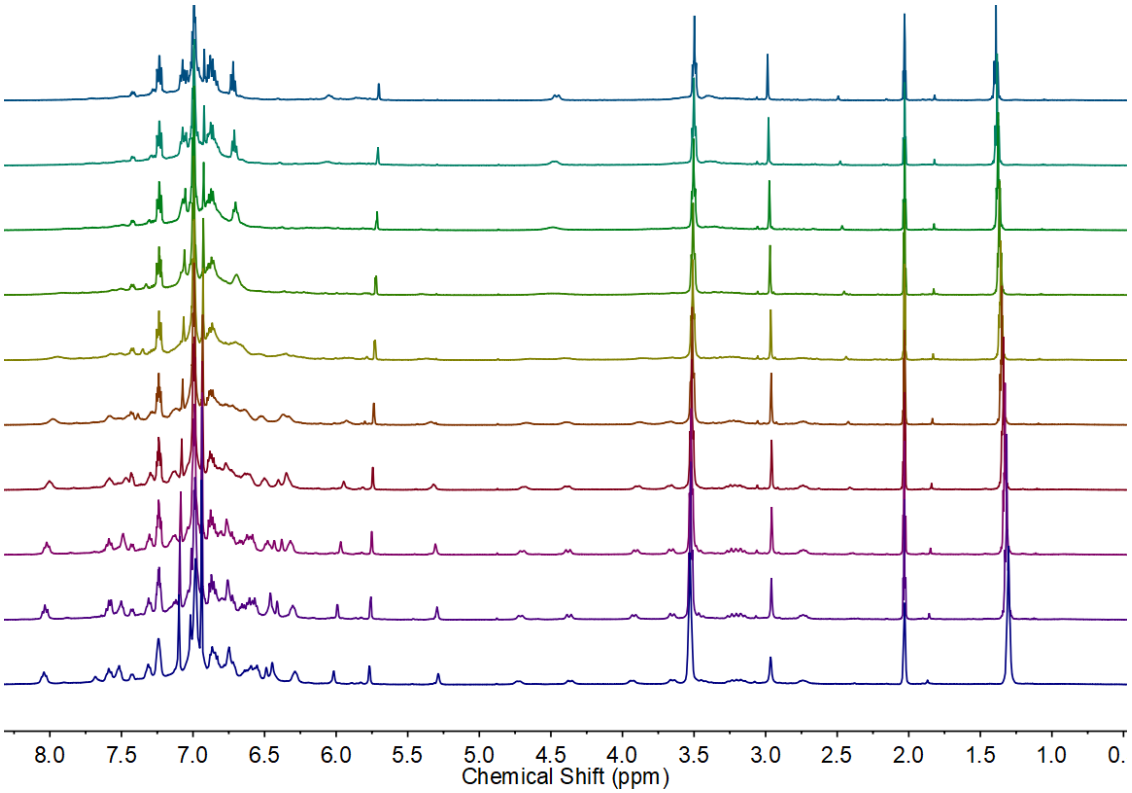

Figure S15: Full variable temperature ^{1}H NMR spectra of **[PNP^{Ph}]$_2$HfCl$_2$** from 203 K to 293 K in 10 K increments (increasing vertically).

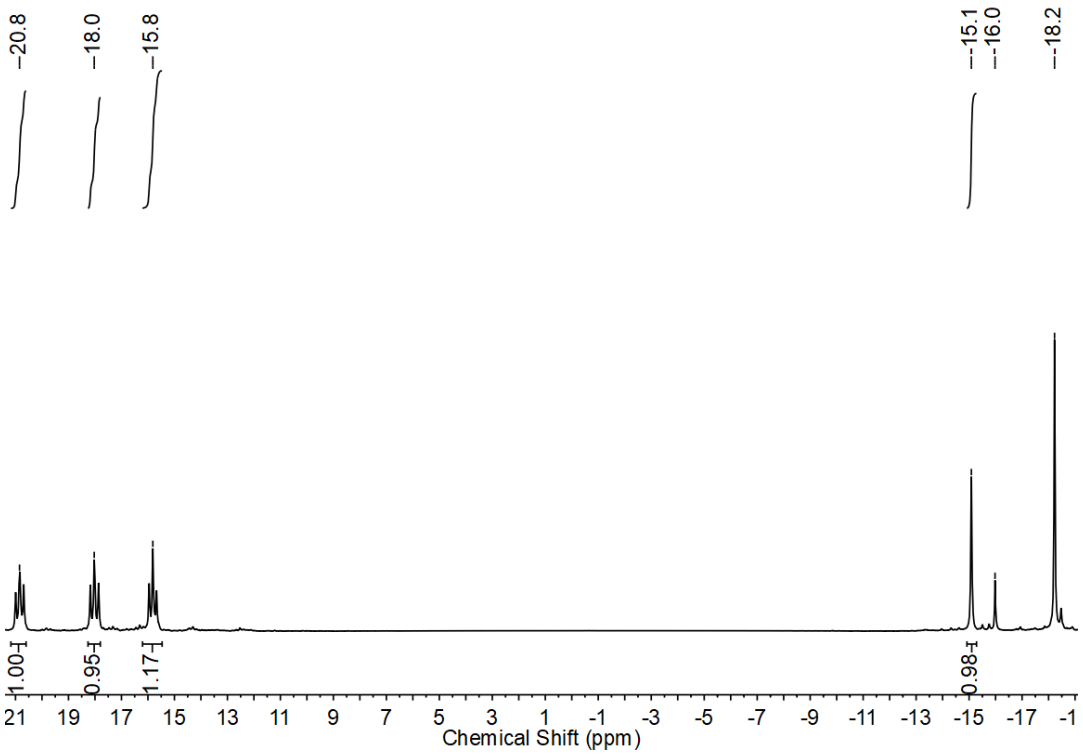

Figure S16: $^{31}P\{^{1}H\}$ NMR spectrum (d^8-toluene) of **[PNP^{Ph}]$_2$HfCl$_2$** at 203 K. The highfield resonances at -15.98 ppm and -18.23 ppm are residual **[PNP^{Ph}]H** and **[PNP^{Ph}]Li·Et$_2$O** respectively.

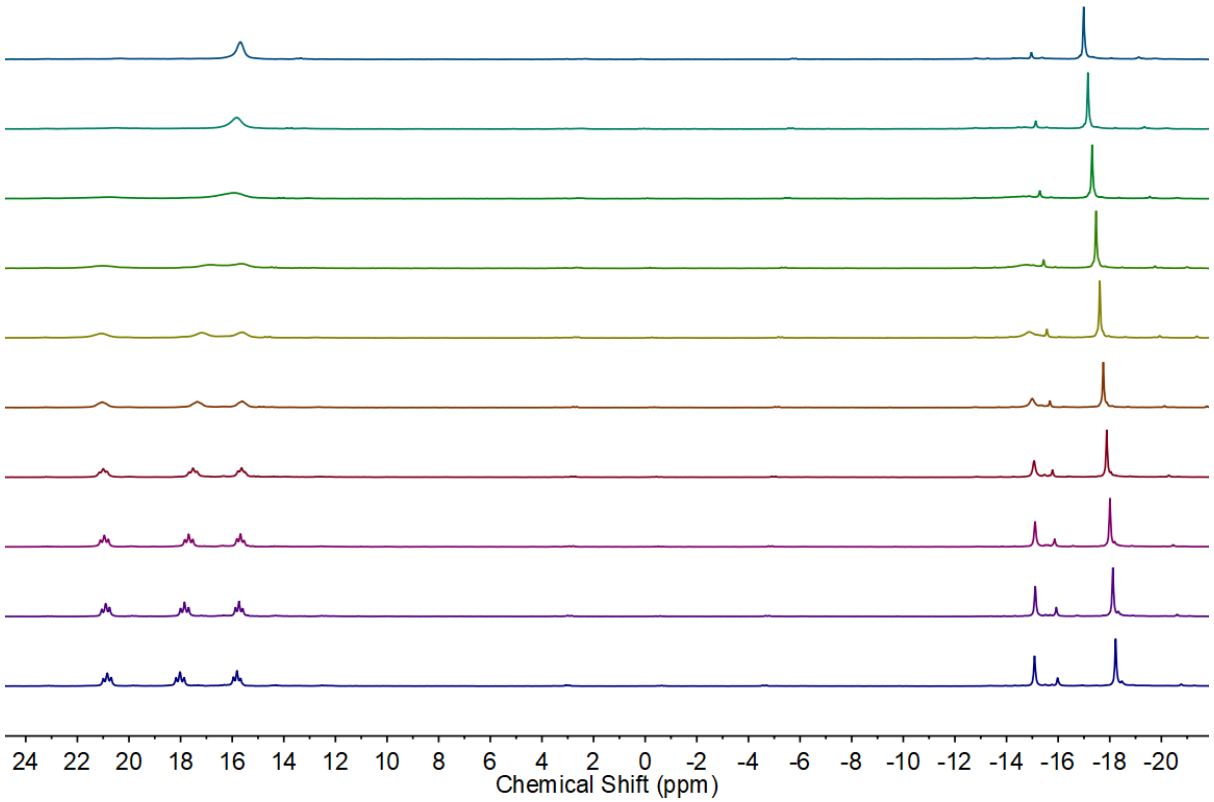

Figure S17: Full variable temperature $^{31}P\{^{1}H\}$ NMR spectra of **[PNP^{Ph}]$_2$HfCl$_2$** from 203 K to 293 K in 10 K increments (increasing vertically).

4 Computational Methods

All electronic structure calculations employed the Gaussian 09 (Revision E.01) program.[18] Initial coordinates of **[PNP^{Ph}]$_2$ZrCl$_2$** were extracted from the experimental single-crystal structure. The PNP^{Ph} ligand was truncated by replacing the phenyl substituents rings of the phosphine donors ligand with methyl groups. Unconstrained geometry optimisations and subsequent frequency calculations of all Zr complexes were carried out at the DFT level, using the BP86 GGA functional.[19,20] The Stuttgart-Dresden SDD effective core potential and associate basis sets were chosen to describe Zr and P atoms,[21] with polarization functions added to P (ζ_d = 0.387)[22] and Zr (ζ_f = 0.875).[23] Pople's 6-31G(d,p) basis set was used on all other atoms (C, N, Cl and H).[24,25] Analysis of the analytical second derivatives of all optimised stationary points confirmed these to be either true minima (positive eigenvalues in the Hessian matrix) or transition states (exactly one imaginary eigenvalue of the Hessian matrix). Minima linked by each transition state were confirmed through subsequent geometry optimizations in both forward and reverse direction of the displacement vector of the transition state coordinate. The frequency calculations also provided thermal and entropic corrections to the total energy in gas phase at T = 298.15 K and p = 1 atm within the rigid-rotor/harmonic oscillator (RRHO) approximation. Effects due to the presence of a solvent were treated implicitly with a polarisable dielectric model, using the IEFPCM formalism in conjunction with Truhlar's SMD model and default parameters for toluene solvent.[26] Single point calculations were performed on the BP86-optimised geometries with BP86,[19,20] B3LYP,[27] BHandHLYP,[28] PBE0,[29] TPSS,[30] TPSSh,[30] CAM-B3LYP,[31] M06,[32,33] M06-L,[32,33] M06-2X[32,33] and **ω**B97M-D3BJ.[34] Dispersion corrections were also applied using Grimme's D3 parameter[35] set on those functionals that do not intrinsically already account for dispersion effects. In all cases the def2-TZVP basis set[36] was used in all single point calculations. Were appropriate (hybrid functionals), calculations made use of the RIJCOSX[37] approximation in conjunction with the def/J auxiliary basis set.[38] in order to increase computational efficiency. All single point calculations were performed with ORCA (version 4.2.1).[39]

5 Computational Results

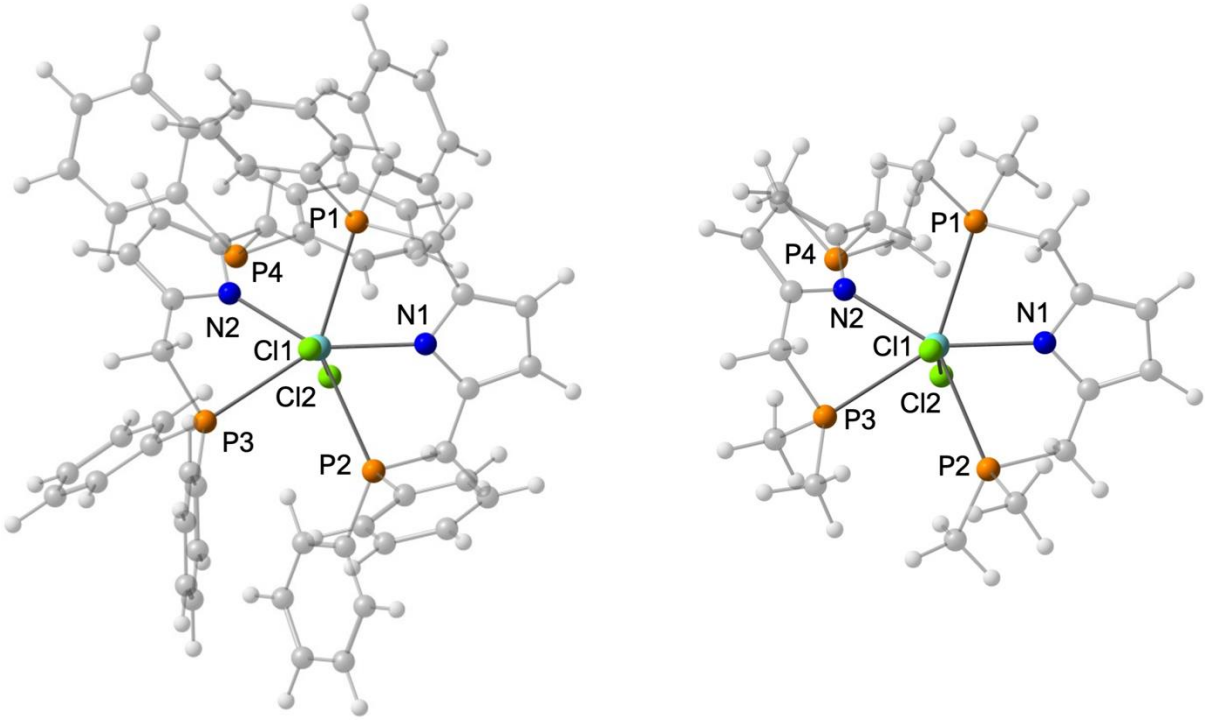

[PNP^{Ph}]$_2$ZrCl$_2$ **[PNP^{Me}]$_2$ZrCl$_2$**

Figure S18: DFT-optimised geometries (BP86/SDD/6-31G(d,p)) of the full model complex **[PNP^{Ph}]$_2$ZrCl$_2$** and its truncated version in which phenyl has been repaced by methyl groups **[PNP^{Me}]$_2$ZrCl$_2$**.

Table S1: Comparison of key optimised and experimental bond parameters (Å, deg) for the full model **[PNP^{Ph}]$_2$ZrCl$_2$** and a truncated version in which phenyl has been repaced by methyl groups **[PNP^{Me}]$_2$ZrCl$_2$**.

	X-Ray	DFT	
		full	*truncated*
Zr(1)–Cl(1)	2.4412(10)	2.461	2.501
Zr(1)–Cl(2)	2.4193(11)	2.467	2.459
Zr(1)–N(1)	2.260(3)	2.278	2.279
Zr(1)–N(2)	2.264(3)	2.268	2.287
Zr(1)–P(1)	2.8267(10)	2.866	2.792
Zr(1)–P(2)	2.7935(10)	2.840	2.778
Zr(1)–P(3)	2.8390(11)	2.883	2.785
Zr(1)–P(4)	4.836(1)	5.028	4.878
Cl(1)–Zr(1)–Cl(2)	170.50(4)	164.76	163.24
P(1)–Zr(1)–N(1)	67.06(9)	67.42	68.70
N(1)–Zr(1)–P(2)	67.96(9)	70.55	70.01
P(2)–Zr(1)–N(2)	81.51(9)	79.69	78.70
N(2)–Zr(1)–P(3)	67.97(9)	68.12	66.97
P(1)–Zr(1)–P(3)	81.20(3)	80.62	80.44

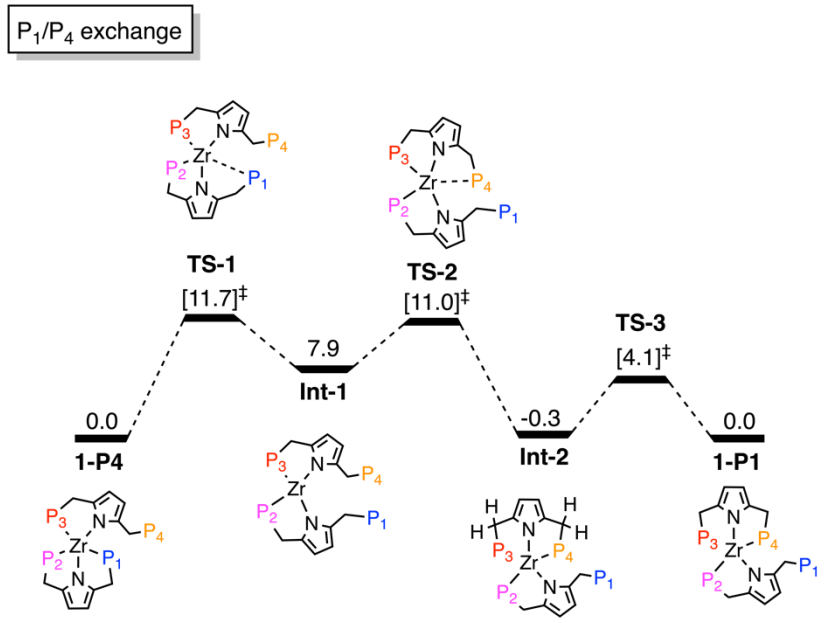

Figure S19: Computed reaction profile (BP86/def2-TZVP corrected for toluene solvent) of the ligand exchange process between **1-P1** and **1-P4**. Relative Gibbs Energies (298 K, 1atm) are given in kcal mol^{-1}.

Table S2. Comparison of relative Free Energies of the ligand exchange process between **1-P1** and **1-P4** in the truncated and full model for a range of functionals. Relative Gibbs Energies (298 K, 1atm) are given in kcal mol^{-1}.

	TS-1	Int-1	TS-2	Int-2	TS-3
$[PNP^{Me}]_2ZrCl_2$					
BP86 (-D3)	11.7 (18.3)	7.9 (16.5)	11.0 (19.2)	–0.3 (0.7)	4.1 (5.7)
B3LYP (–D3)	9.4 (16.2)	5.3 (13.2)	8.8 (16.3)	–0.5 (0.2)	4.1 (5.2)
TPSS (–D3)	13.2 (17.8)	9.3 (15.3)	12.6 (18.3)	–0.6 (0.1)	3.9 (5.0)
TPSSh (–D3)	14.0 (18.4)	9.9 (15.8)	13.4 (19.0)	–0.6 (0.0)	4.0 (5.1)
BHLYP (–D3)	11.9 (17.5)	7.4 (14.2)	11.3 (17.6)	–0.7 (–0.3)	4.1 (5.0)
PBE0 (–D3)	15.0 (18.1)	11.0 (15.4)	14.4 (18.6)	–0.3 (0.1)	4.3 (5.2)
CAM-B3LYP (–D3)	12.8 (16.6)	8.5 (13.2)	12.2 (16.7)	–0.5 (0.0)	4.1 (5.1)
M06–L	17.3	13.0	16.7	–0.1	5.1
M06	16.1	12.6	15.5	0.6	5.8
M06–2X	17.6	13.3	17.0	0.2	4.7
ωB97M–D3BJ	17.7	13.5	17.1	–0.1	4.6
$[PNP^{Ph}]_2ZrCl_2$					
BP86 (-D3)	4.9 (24.5)	0.9 (20.8)	6.1 (24.7)	0.5 (2.9)	
B3LYP (–D3)	2.2 (19.8)	–2.6 (15.2)	3.1 (20.0)	0.2 (2.3)	
TPSS (–D3)	7.2 (21.7)	3.0 (17.6)	8.3 (22.0)	0.5 (2.3)	
TPSSh (–D3)	8.1 (22.5)	3.6 (18.1)	9.2 (22.7)	0.6 (2.3)	
BHLYP (–D3)	5.7 (19.9)	0.0 (14.3)	6.6 (20.2)	0.5 (2.0)	
PBE0 (–D3)	10.0 (20.9)	5.0 (16.0)	10.8 (21.0)	0.9 (2.1)	
CAM-B3LYP (–D3)	7.2 (19.1)	1.7 (13.7)	8.1 (19.1)	0.6 (1.9)	

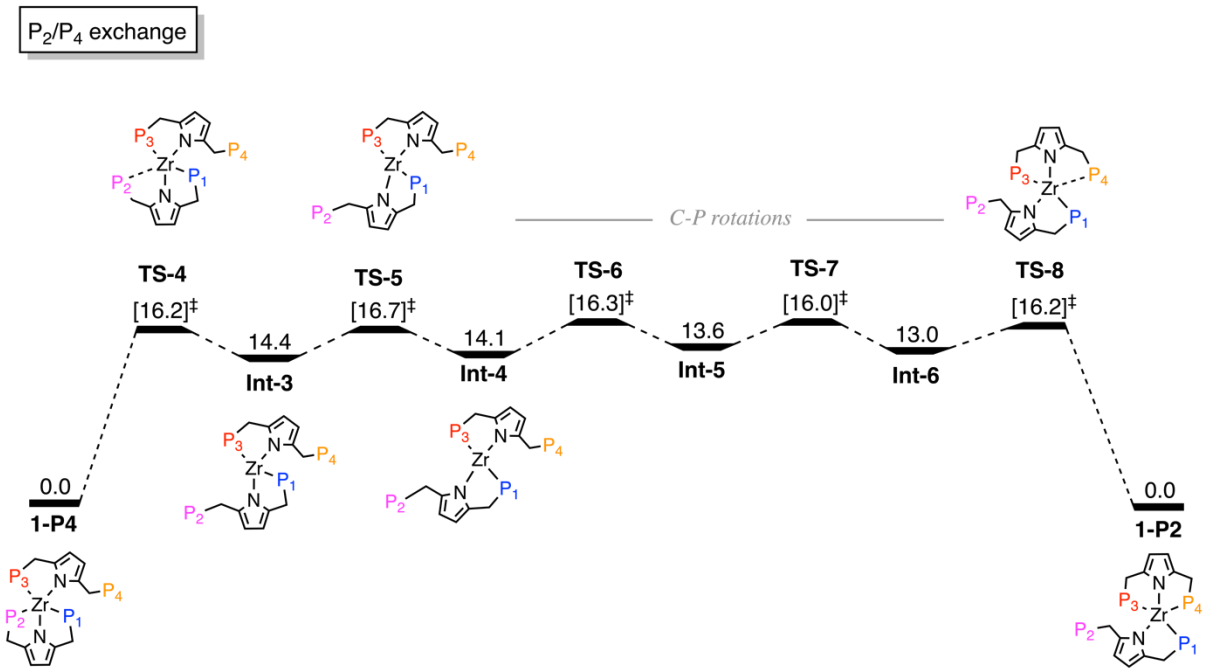

Figure S18: Computed reaction profile (BP86/def2-TZVP corrected for toluene solvent) of the ligand exchange process between **1-P2** and **1-P4**. Relative Gibbs Energies (298 K, 1atm) are given in kcal mol^{-1}.

Table 3: Comparison of relative Free Energies of the ligand exchange process between **1-P2** and **1-P4** for a range of functionals. Relative Gibbs Energies (298 K, 1atm) are given in kcal mol^{-1}.

	TS-4	**Int-3**	**TS-5**	**Int-4**	**TS-6**	**Int-5**	**TS-7**	**Int-6**	**TS-8**
BP86 (-D3)	16.2 (26.6)	14.4 (24.4)	16.7 (27.7)	14.1 (23.7)	16.3 (27.1)	13.6 (23.1)	16.0 (26.7)	13.0 (22.6)	16.2 (26.6)
B3LYP (–D3)	14.1 (23.5)	12.4 (21.4)	13.3 (23.5)	12.1 (20.7)	13.8 (23.5)	11.2 (19.9)	13.7 (23.5)	11.1 (19.8)	14.1 (23.5)
TPSS (–D3)	18.2 (25.5)	16.5 (23.4)	18.3 (26.0)	16.1 (22.7)	18.1 (25.5)	15.0 (21.5)	17.5 (24.9)	14.9 (21.6)	18.2 (25.5)
TPSSh (–D3)	19.0 (26.2)	17.3 (24.0)	19.1 (26.6)	16.8 (23.3)	18.9 (26.2)	15.7 (22.0)	18.4 (25.6)	15.7 (22.2)	19.0 (26.2)
BHLYP (–D3)	16.8 (24.8)	15.0 (22.7)	15.5 (24.0)	14.5 (21.8)	16.2 (24.4)	13.2 (20.6)	16.4 (24.6)	13.6 (21.0)	16.8 (24.8)
PBE0 (–D3)	20.2 (25.5)	18.3 (23.4)	20.5 (26.1)	17.8 (22.6)	20.0 (25.5)	16.8 (21.5)	19.9 (25.2)	16.7 (21.6)	20.2 (25.5)
CAM-B3LYP (–D3)	17.6 (23.5)	15.7 (21.3)	17.1 (23.1)	15.1 (20.6)	17.1 (23.2)	14.2 (19.4)	17.2 (23.1)	14.3 (19.7)	17.6 (23.5)
M06–L	23.6	21.3	22.7	20.3	23.1	18.5	22.8	19.3	23.6
M06	22.7	20.7	22.9	19.8	23.0	18.8	23.0	18.7	22.7
M06–2X	23.2	21.2	22.9	19.8	22.9	18.7	22.8	19.1	23.2
ωB97M–D3BJ	23.5	21.6	23.9	20.5	23.3	19.4	23.3	19.8	23.5

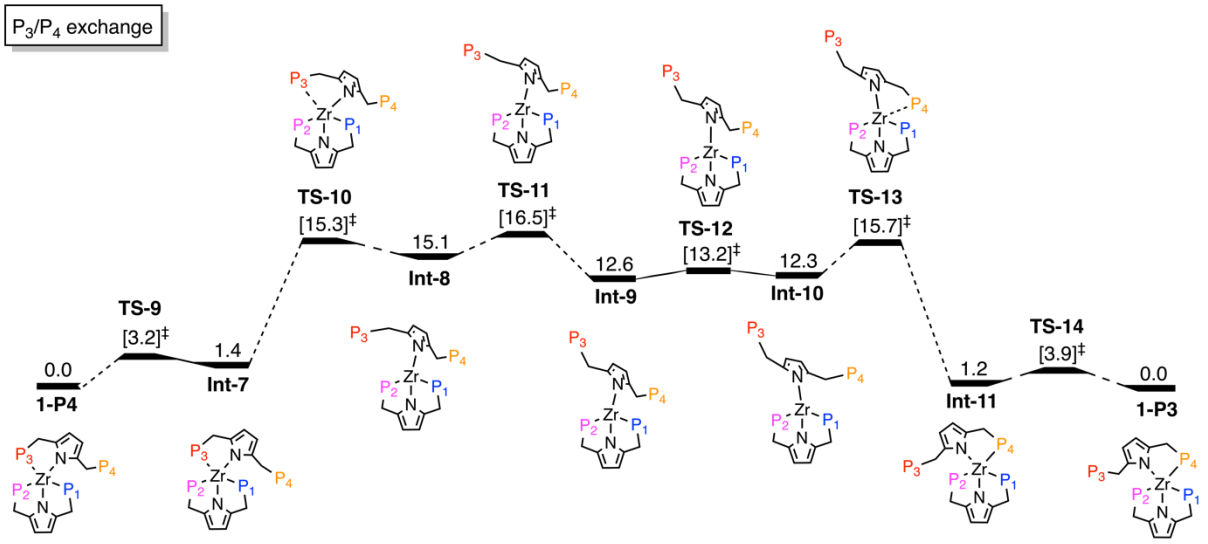

Figure S21: Computed reaction profile (BP86/def2-TZVP corrected for toluene solvent) of the ligand exchange process between **1-P3** and **1-P4**. Relative Gibbs Energies (298 K, 1atm) are given in kcal mol^{-1}.

Table 4. Comparison of relative Free Energies of the ligand exchange process between **1-P3** and **1-P4** for a range of functionals. Relative Gibbs Energies (298 K, 1atm) are given in kcal mol^{-1}.

	TS-9	**Int-7**	**TS-10**	**Int-8**	**TS-11**	**Int-9**
BP86 (-D3)	3.2 (4.5)	1.4 (2.6)	15.3 (22.2)	15.1 (23.0)	16.5 (25.4)	12.6 (21.2)
B3LYP (–D3)	3.3 (4.3)	1.3 (2.2)	14.3 (20.7)	14.1 (21.4)	15.4 (23.6)	11.2 (19.3)
TPSS (–D3)	3.1 (3.8)	1.3 (2.0)	17.2 (22.1)	16.8 (22.3)	17.8 (24.1)	13.9 (19.8)
TPSSh (–D3)	3.1 (3.9)	1.2 (2.0)	18.0 (22.7)	17.5 (23.0)	18.6 (24.7)	14.7 (23.0)
BHLYP (–D3)	3.3 (4.1)	1.1 (1.8)	16.7 (22.1)	16.9 (23.0)	18.1 (25.1)	14.2 (21.0)
PBE0 (–D3)	3.3 (3.9)	1.3 (1.9)	18.6 (22.2)	18.6 (22.6)	19.9 (24.4)	16.1 (20.4)
CAM-B3LYP (–D3)	3.3 (4.0)	1.2 (1.9)	17.3 (21.1)	17.5 (21.8)	18.8 (23.8)	15.0 (19.6)
M06–L	3.3	2.1	18.8	19.3	21.5	17.4
M06	3.6	1.9	17.9	18.3	20.8	16.8
M06–2X	3.8	2.0	18.9	19.9	22.5	18.5
ωB97M–D3BJ	3.6	1.7	21.0	21.7	23.4	19.6
	TS-12	**Int-10**	**TS-13**	**Int-11**	**TS-14**	
BP86 (-D3)	13.2 (22.2)	12.3 (20.4)	15.7 (25.6)	1.2 (0.8)	3.9 (5.1)	

B3LYP (–D3)	10.8 (19.2)	10.2 (19.7)	13.6 (22.6)	1.1 (0.7)	4.0 (5.0)	
TPSS (–D3)	14.9 (21.0)	13.6 (19.0)	17.3 (24.0)	1.0 (0.5)	3.9 (4.7)	
TPSSh (–D3)	15.7 (21.6)	14.3 (19.5)	18.1 (24.7)	1.0 (0.5)	4.0 (4.8)	
BHLYP (–D3)	13.0 (20.2)	12.2 (18.6)	16.1 (23.7)	1.0 (0.7)	4.4 (5.2)	
PBE0 (–D3)	16.6 (21.0)	15.3 (19.1)	19.4 (24.3)	0.9 (0.6)	4.4 (5.0)	
CAM-B3LYP (–D3)	14.3 (19.1)	13.0 (17.4)	16.9 (22.3)	1.0 (0.6)	4.3 (4.9)	
M06–L	17.8	16.1	21.8	0.1	5.1	
M06	17.5	16.5	22.3	0.6	5.6	
M06–2X	18.6	16.8	21.9	0.7	5.3	
ωB97M–D3BJ	19.5	17.4	22.3	0.5	4.9	

6 References

1 Oxford Diffraction Ltd., 2011.

2 L. Palatinus and G. Chapuis, *J. Appl. Crystallogr.*, 2007, **40**, 786–790.

3 P. W. Betteridge, J. R. Carruthers, R. I. Cooper, K. Prout and D. J. Watkin, *J. Appl. Crystallogr.*, 2003, **36**, 1487–1487.

4 R. I. Cooper, A. L. Thompson and D. J. Watkin, *J. Appl. Crystallogr.*, 2010, **43**, 7.

5 L. E. Manxzer, J. Deaton, P. Sharp and R. R. Schrock, in *Inorganic Syntheses*, John Wiley & Sons, Inc., 2007, pp. 135–140.

6 I. T. Kim and R. L. Elsenbaumer, *Tetrahedron Lett.*, 1998, **39**, 1087–1090.

7 D. S. Levine, T. D. Tilley and R. A. Andersen, *Organometallics*, 2015, **34**, 4647–4655.

8 S. Kuriyama, K. Arashiba, K. Nakajima, H. Tanaka, K. Yoshizawa and Y. Nishibayashi, *Eur. J. Inorg. Chem.*, 2016, **2016**, 4856–4861.

9 A. L. Narro, H. D. Arman and Z. J. Tonzetich, *Organometallics*, 2019, **38**, 1741–1749.

10 R. Kawakami, S. Kuriyama, H. Tanaka, K. Arashiba, A. Konomi, K. Nakajima, K. Yoshizawa and Y. Nishibayashi, *Chem. Commun.*, 2019, **55**, 14886–14889.

11 S. Kuriyama, K. Arashiba, H. Tanaka, Y. Matsuo, K. Nakajima, K. Yoshizawa and Y. Nishibayashi, *Angew. Chemie Int. Ed.*, 2016, **55**, 14291–14295.

12 Y. Sekiguchi, S. Kuriyama, A. Eizawa, K. Arashiba, K. Nakajima and Y. Nishibayashi, *Chem. Commun.*, 2017, **53**, 12040–12043.

13 Y. Sekiguchi, F. Meng, H. Tanaka, A. Eizawa, K. Arashiba, K. Nakajima, K. Yoshizawa and Y. Nishibayashi, *Dalt. Trans.*, 2018, **47**, 11322–11326.

14 J. A. Kessler and V. M. Iluc, *Inorg. Chem.*, 2014, **53**, 12360–12371.

15 M. Kreye, M. Freytag, P. G. Jones, P. G. Williard, W. H. Bernskoetter and M. D. Walter,

Chem. Commun., 2015, **51**, 2946–2949.

16 N. Ehrlich, M. Kreye, D. Baabe, P. Schweyen, M. Freytag, P. G. Jones and M. D. Walter, *Inorg. Chem.*, 2017, **56**, 8415–8422.

17 N. Ehrlich, D. Baabe, M. Freytag, P. G. Jones and M. D. Walter, *Polyhedron*, 2018, **143**, 83–93.

18 Gaussian 09 (Revision E.01), M. J. Frisch, G. W. Trucks, H. B. Schlegel, G. E. Scuseria, M. A. Robb, J. R. Cheeseman, G. Scalmani, V. Barone, G. A. Petersson, H. Nakatsuji, X. Li, M. Caricato, A. Marenich, J. Bloino, B. G. Janesko, R. Gomperts, B. Mennucci, H. P. Hratchian, J. V. Ortiz, A. F. Izmaylov, J. L. Sonnenberg, D. Williams-Young, F. Ding, F. Lipparini, F. Egidi, J. Goings, B. Peng, A. Petrone, T. Henderson, D. Ranasinghe, V. G. Zakrzewski, J. Gao, N. Rega, G. Zheng, W. Liang, M. Hada, M. Ehara, K. Toyota, R. Fukuda, J. Hasegawa, M. Ishida, T. Nakajima, Y. Honda, O. Kitao, H. Nakai, T. Vreven, K. Throssell, J. A. Montgomery, Jr., J. E. Peralta, F. Ogliaro, M. Bearpark, J. J. Heyd, E. Brothers, K. N. Kudin, V. N. Staroverov, T. Keith, R. Kobayashi, J. Normand, K. Raghavachari, A. Rendell, J. C. Burant, S. S. Iyengar, J. Tomasi, M. Cossi, J. M. Millam, M. Klene, C. Adamo, R. Cammi, J. W. Ochterski, R. L. Martin, K. Morokuma, O. Farkas, J. B. Foresman, and D. J. Fox, Gaussian, Inc., Wallingford CT, 2013.

19 A. D. Becke, *Phys. Rev. A*, 1988, **38**, 3098–3100.

20 J. P. Perdew, *Phys. Rev. B*, 1986, **33**, 8822–8824.

21 D. Andrae, U. Haussermann, M. Dolg, H. Stoll and H. Preuss, *Theor. Chim. Acta.*, 1990, **77**, 123–141.

22 A. Hollwarth, M. Bohme, S. Dapprich, A. W. Ehlers, A. Gobbi, V. Jonas, K. F. Kohler, R. Stegmann, A. Veldkamp and G. Frenking, *Chem. Phys. Lett.*, 1993, **208**, 237–240.

23 A. W. Ehlers, M. Bohme, S. Dapprich, A. Gobbi, A. Hollwarth, V. Jonas, V., K. F. Kohler, R. Stegmann, A. Veldkamp and G. Frenking, *Chem. Phys. Lett.*, 1993, **208**, 111–114.

24 W. J. Hehre, R. Ditchfield and J. A. Pople, *J. Chem. Phys.*, 1972, **56**, 2257–2261.

25 P. C. Harihara and J. A. Pople, *Theor. Chim. Acta*, 1973, **28**, 213–222.

26 A. V. Marenich, C. J. Cramer and D. G. Truhlar, *J. Phys. Chem. B*, 2009, **113**, 6378–6396.

27 P. J. Stephens, F. J. Devlin, C. F. Chabalowski and M. J. Frisch, *J. Phys. Chem*., 1994, **98**, 11623−11627.

28 A. D. Becke, *J. Chem. Phys.*, 1993, **98**, 1372–1377.

29 C. Adamo and V. Barone, *J. Chem. Phys.*, 1999, **110**, 6158–6169.

30 J. Tao, J. P. Perdew, V. N. Staroverov and G. E. Scuseria, *Phys. Rev. Lett*., 2003, **91**, 146401.

31 T. Yanai, D. P. Tew and N. C. Handy, *Chem. Phys. Lett*., 2004, **393**, 51−57.

32 Y. Zhao, and D. G. Truhlar, *J. Chem. Phys*., 2006, **125**, 194101.

33 Y. Zhao and D. G. Truhlar, *Theor. Chem. Acc.*, 2008, **120**, 215–241.

34 A. Najibi, and L. Goerigk, *J. Chem. Theory Comput*., 2018, **14**, 5725−5738.

35 S. Grimme, J. Antony, S. Ehrlich and H. Krieg, *J. Chem. Phys.*, 2010, **132**, 154104.

36 F. Weigend and R. Ahlrichs, *Phys. Chem. Chem. Phys*., 2005, **7**, 3297–3305.

37 F. Neese, F. Wennmohs, A. Hansen and U. Becker, *Chem. Phys*., 2009, **356**, 98–109.

38 F. Weigend, *Phys. Chem. Chem. Phys.*, 2006, **8**, 1057–1065.

39 F. Neese, *Wiley Interdiscip. Rev. Comput. Mol. Sci.,* 2017, **8**, e1327.